ORB ACADEMIC PUBLISHER

Int. J. Eng. Math. Model., vol. 2016, p. 27-42
Available online at www.orb-academic.org

International Journal of Engineering and Mathematical Modelling
ISSN: 2351-8707

A Mathematical Model for Study of Cyclic Purge in Vessels with Complex Geometry

Jivaan Kishore[1,•], Farhang Shadman[1]

[1] *Department of Chemical and Environmental Engineering – University of Arizona, Tucson, Arizona 85721*
Email: jivaankj@email.arizona.edu
[•] *Corresponding author.*

ABSTRACT
Removal of impurities from stagnant regions in process vessels and flow components is a major bottleneck of purge operations and typically associated with large downtimes and UHP gas consumption. A comprehensive mathematical model is developed for study of the purge process in chambers with complex geometry and stagnant regions inaccessible to gas flow. The model takes into account the dynamics of removing impurities in the gas phase as well as those adsorbed on the chamber surfaces. Using this model, the conventional Steady State Purge (SSP) is compared with a proposed unsteady Pressure Cyclic Purge (PCP) technique. PCP is found to be advantageous over SSP in terms of gas usage and purge time required to reach a given target cleanliness. The effects of a number of key design and operational parameters such as chamber geometry, pressure range, and cycling pattern are investigated. The results show that the model is a powerful tool for finding the optimum operating conditions for purging a system.

KEYWORDS
Purge process — Contamination control — Computational Fluid Dynamics — Transport processes

1. Introduction

Gas-phase purging is often used for removing impurities from gas delivery systems as well as processing chambers and equipment. For example, the drying down of gas distribution systems and process tools is common during semiconductor manufacturing. Contamination control is becoming very time consuming and resource intensive as required cleanliness increases. Electronics industries encounter relatively large tool downtimes and expensive ultra-high purity (UHP) gas consumption owing to the parts per billion (ppb) to parts per trillion (ppt) level of purity required in some operations. In such cases developing and implementing optimized purge scenarios become critical for product quality and throughput. Conventional purge processes usually require large tool downtimes and high cost of operation. Therefore, the need for cost-effective purge techniques is ever increasing [1].

Studies on conventional Steady-State Purge (SSP) on gas distribution lines pertaining to moisture as a contaminant have been carried out [2]-[5]. During SSP operation, a steady flow of UHP gas is maintained through the system, whereas during Pressure Cyclic Purge (PCP), the system is cycled between high and low pressures. In a typical depressurization step, the UHP inlet flow is reduced or shut off to let gas trapped in the system to escape to an external environment at a lower pressure, thus lowering the system pressure. In a subsequent pressurization step, UHP gas is reintroduced by ramping up the inlet flow rate.

The benefits of the PCP approach for the drying of simple electro-polished stainless steel distribution systems have been previously reported [6]. The application of conventional and cyclic purging in the drying down of UHP gas distribution systems has also been studied and the enhancement of purge performance and attaining high purge rates using pressure cyclic purge (PCP) has been demonstrated [7]. Moreover, related studies have shown the disadvantages of using a vacuum in purging operations due to the risk of back diffusion of impurities into UHP systems [8]-[9].

Similar to delivery lines in UHP environments, dead spaces in mass-flow controllers, gauges, valves, and process chambers are areas that receive little or no direct flow. The only mechanism of contaminant outgassing from these areas during conventional high pressure purging is by surface desorption and slower process of diffusion. Hence a comprehensive purge simulator is needed to understand and compare different purge techniques. This would further result in an overall process cost reduction and environmental safety and health (ESH) gains by reducing process gas and energy usage.

Optimizing the purge operating conditions through experimental means can be cumbersome and impractical for complex systems considering the large number of operational parameters and configurations that need to be taken in to account. Hence, an efficient computational approach to simulate the purge process is very valuable. This work presents the development of such a mathematical tool and the application of it for analysis of purging of contaminants in process chambers.

2. Model development

2.1 Base-Case Conditions

A cubical chamber geometry with dead spaces located on top and bottom, as shown in Figure 1b, was chosen as the base-case geometry. The system consisted of inlet and outlet pipes located at opposite sides of the chamber. The dead spaces were located such that they would receive negligible short-cut direct gas flow between the inlet and outlet. A variable flow restrictive orifice cycling between a maximum valve loss coefficient of 1E8 for pressurization and minimum of 1E3 for depressurization is used at the outlet to control the pressure ramp rate in the system. In a conventional steady-state purge, the system is maintained at a constant high pressure of 7.5E5 Pa by throttling flow by means of a mass flow controller upstream of the inlet to 2.5E5 sccm. During PCP the system is cycled between base case high and low pressures of 7.5E5 Pa and 2.5E5 Pa respectively realized by cycling mass flow rate. An initially pressurized system is allowed to depressurize by shutting off the mass flow and re-pressurized by ramping up to 2.5E5 sccm. The system is maintained in the shut off and high mass flow states for 120 s each to reach the desired base pressures. These values for cycle time and pressure levels depend on the outlet valve coefficient and chamber geometry. Hence they need to be reevaluated on a case by case basis. The different transport mechanisms involved in a purge process is shown in Figure 1a.

The chamber is initially filled with nitrogen gas of a uniform moisture concentration of $1.71E-5\ mol/m^3$ (420 ppb at atmospheric pressure). The internal surfaces are assumed to be in equilibrium with the gas phase moisture before the start of the purge process. Purging is carried out with UHP Nitrogen gas with a moisture concentration of $8.2E-9\ mol/m^3$ (0.2 ppb).

2.2 Governing Equations

A comprehensive mathematical model is developed in order to simulate and analyze the purge characteristics in three-dimensional space. The model consists of fluid dynamics, mass transport in the gas phase, and surface species interactions and takes into account the dynamics of various modes of impurity transport. Reducing surface contamination is the primary goal of the chamber purge process. Contaminant desorption from the surface is a process of high activation energy and controls the extent of purge. In a typical purge process the introduction of UHP gas enables contaminants to desorb from the surface, and then be effectively removed via convection. Simultaneous solution of continuity and momentum balance equations provides a complete picture of pressure and gas velocity fields in the system. Fully compressible flow assumption is used to capture changes in gas density with pressure. The single-phase Newtonian model governing gas dynamics is given by the following equations [10]:

$$\rho\frac{\partial u}{\partial t}+\rho(u.\nabla)u=-\nabla p+\mu\nabla^2u-\nabla.\left[\frac{2}{3}\mu(\nabla.u)\right] \tag{2.1}$$

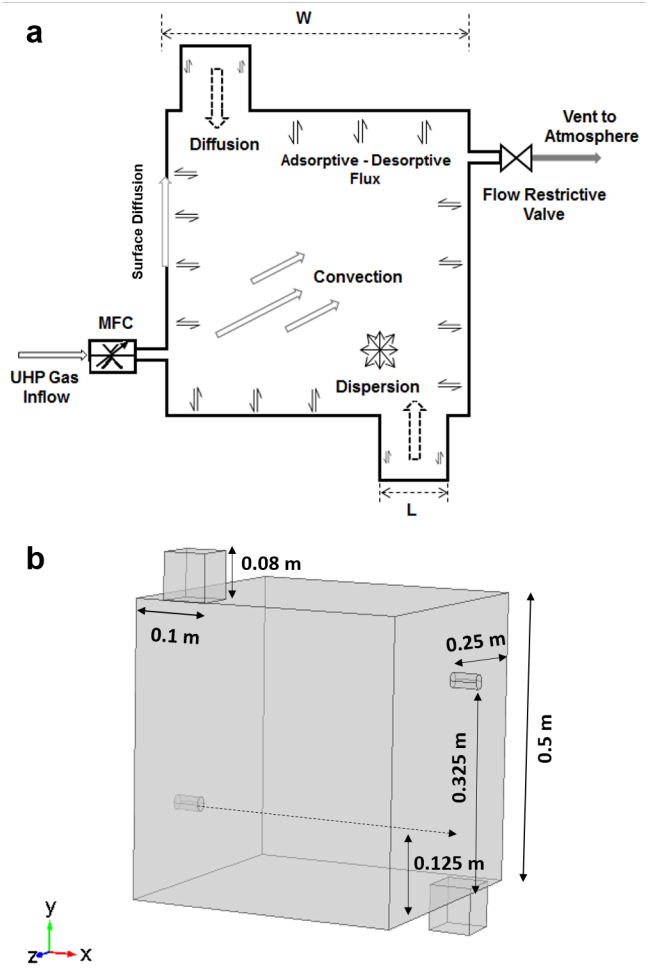

Figure 1. *a) Impurity transport mechanisms, b) 3D chamber schematic*

$$\frac{\partial \rho}{\partial t} + \nabla.(\rho u) = 0 \tag{2.2}$$

The Navier Stokes Equation (2.1), written for Newtonian fluids, relates the fluid kinetic energy to normal shear forces. In this equation the two terms on the right-hand side $-\mu\nabla^2 u - \nabla.\left[\frac{2}{3}\mu(\nabla.u)\right]$ represent the totality of viscous stresses known as the viscous stress tensor. The term $\mu\nabla^2 u$ is the viscous strain rate, representing the viscous deformation forces on a material packet in a fluid stream. The values for density and viscosity in this study are those of nitrogen at room temperature and varying system pressure.

The transport of chemical species in the bulk is given by the following equation:

$$\frac{\partial C_g}{\partial t} + u.\nabla C_g = \nabla.(D_e \nabla C_g) \tag{2.3}$$

where, C_g is the gas phase concentration and u is the velocity vector at a given point in space and time, derived from the solution of Equations (2.1) and (2.2). In addition to the convective flux, there is dispersive flux due to combined effects of molecular motion as well as eddies generated by the large spatial and temporal variations of the local velocity, pressure, and fluid properties due to cyclic transience. To the best of our knowledge, there is no

data or correlation in the literature for dispersion under PCP conditions similar to those in this study. In fact, the common measures of flow regimes, such as Reynolds number, are not applicable due to sharp pressure changes in the flow condition. In our previous study we found that the following empirical equation for the average local dispersion under similar conditions gave a good agreement with the experimental data [7]:

$$D_e = D_{mp} + apu^2 \tag{2.4}$$

where D_e represents isotropic effective dispersion coefficient, D_m is the molecular diffusivity and a is a fit parameter. The dependence of molecular diffusivity on pressure is given by Chapman-Enskog equation as follows [11]:

$$D_{mp} = \frac{D_m P_{atm}}{p} \tag{2.5}$$

A conservative form of convective term is used in order to capture and convey the effects of sharp changes in system pressure and resulting gas velocity. This is critical during pressure cycling steps in order to account for concentration changes during pressurization and depressurization.

A first order adsorption-desorption equation is used to model the flux balance at the surfaces. The initial contaminant surface concentration ($6.3E-6 mol/m^2$) is lower than the evaluated surface site density of 316L EPSS ($1E-5 mol/m^2$). Hence, the maximum moisture coverage is less than a mono-layer and hence is well represented by a first-order adsorption desorption expression. The maximum moisture concentration in the chamber throughout the process is below $500 ppb$, further justifying the use of the Langmuir-type kinetics [12]. The conservation equation for contaminant adsorbed on the surface is given by the following equation:

$$\frac{\partial C_s}{\partial t} = \nabla.(D_s \nabla C_s) + k_a C_g (S_0 - C_s) - k_d C_s \tag{2.6}$$

where C_s is the surface concentration of the contaminant species, S_0 is the total available active site density, D_s is the surface diffusivity of contaminant on the chamber surface, and k_a, k_d are the adsorption and desorption rate coefficients.

The chamber surface in this case is assumed to be 316L EPSS (Low carbon Austenitic electro polished stainless steel alloy containing 2% to 3% Molybdenum apart from Ni, Cr). Although the surface diffusive flux is much lower in magnitude compared to other fluxes, its addition as a second order term to the model acts as a numerical stabilizer.

2.3 Boundary and Initial Conditions

The chamber is assumed to be initially pressurized with no UHP gas flow through it. The initial contaminant concentration in the gas phase is assumed to be uniform; the concentration on the chamber surfaces is also uniform and in equilibrium with the gas phase. The initial conditions are given as follows:

$$p = P_{atm} \tag{2.7}$$

$$u = 0 \tag{2.8}$$

$$C_g = C_{gi} \tag{2.9}$$

$$C_s = C_{s0} = \frac{k_a C_{gi} S_0}{k_d + k_a C_{gi}} \tag{2.10}$$

As described before, the chamber consists of an inlet for UHP gas introduction and an outlet whose opening is controlled through a valve for venting to atmosphere. Pressure cycling is accomplished by synchronous valve and mass flow control operations. The inlet boundary condition for mass flow rate is given as follows:

$$Q_{in} = -\int \frac{\rho}{\rho_{st}(u.n)(d)} dS \tag{2.11}$$

$$P_{st} = \frac{P_{st} M_n}{R T_{st}} \tag{2.12}$$

where, dS is the differential surface area over the boundary's cross section, n is the outward pointing unit normal vector, ρ_{st} is the density of the gas at standard pressure P_{st} (101 kPa) and standard temperature T_{st} (273 K). d represents the inlet pipe diameter, R is the universal gas constant and M_n (0.028 kg/mol) is the molecular weight of Nitrogen. Integral mass flow rate across the inlet boundary is specified by a periodic function. The time periods in the function refer to the pressurization and depressurization times. These periods depend on a combination of factors including system geometry and flow restrictive device properties. The tangential velocity at the inlet is zero and the mass flow is normal to the boundary. The pressure at the outlet boundary is expressed as by the following valve equation [13]:

$$p = P_{atm} + 0.5 K_f \rho u^2 \tag{2.13}$$

where K_f is the valve loss coefficient describing the extent of valve opening or closure and P_{atm} is the atmospheric pressure. The valve loss coefficient is cycled at the outlet in conjunction with the mass flow rate at the inlet to obtain the desired rate of pressurization and depressurization. In SSP the system is kept at a constant gas flow and a pressure equal to the high pressure level of PCP.

Since throttling the mass flow is more practical in an industrial setup, a mass-flow boundary condition is used for the inlet. The input mass flow and valve coefficient cycles as functions of time are shown in Figure 2.

On the chamber walls, the velocity is zero and the adsorption and desorption dynamics are given by Langmuir-type expression. Therefore, the flux balance at the wall is given as follows:

$$-n.(-D_e \nabla C_g + u C_g) = k_d C_s - k_a C_g (S_0 - C_s) \tag{2.14}$$

Following are the boundary conditions for the above governing equations, assuming that the inlet is at the baseline purge gas concentration, the outlet is dominated by convection, and the surface fluxes of adsorbed molecules at both inlet and outlet are negligible:

$$C_g = C_{g\,in} \tag{2.15}$$

$$-n.D_e \nabla C_g = 0 \tag{2.16}$$

$$\nabla C_s = 0 \tag{2.17}$$

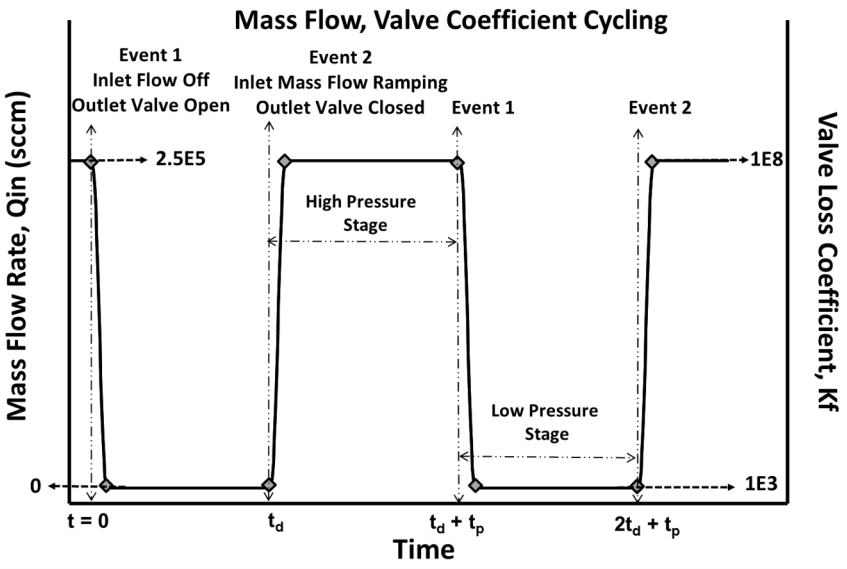

Figure 2. *Typical inlet mass flow and outlet valve coefficient cycling profile*

2.4 Solver and Meshing

The described mathematical model was solved using a finite element method . The simultaneous solution to the above set of equations provided the spatial and temporal values of pressure, velocity, gas and surface concentrations in a three-dimensional geometry of the chamber.

Considering the highly non-linear nature of the coupled equations, choice of stabilization method as well as selection of mesh type, size, and distribution were not routine or trivial. A relatively dense mesh distribution was used around inlet, outlet, and corner regions. Distribution of mesh elements and varying density in the front, side, and bottom of the 3D chamber is shown in Figure 3. Various mesh pattern choices and refinements were carried out make sure that results were independent of the choice of these computational mesh factors.

3. Results and Discussion

3.1 Model Validation and Parameter Estimation

The fundamental rate coefficients for adsorption and desorption (k_a, k_d) and the surface site density (S_0) for moisture interactions with 316L EPSS pipes were obtained by fitting the model to data obtained in a previous study dealing with PCP process in pipes, as shown in Figure 4 [14]. Table 1 is a list of the fundamental input parameters obtained by this data fitting.

Parameter	Fitted value
$k_a\ [m^3/(mol*s)]$	$7.1E3$
$k_d\ [1/s]$	$3.78E-4$
$S_0[mol/m^2]$	$1E-5$
$a\ [kg/(m*s^2)]$	$5.06E-4$

Table 1. Input model parameters

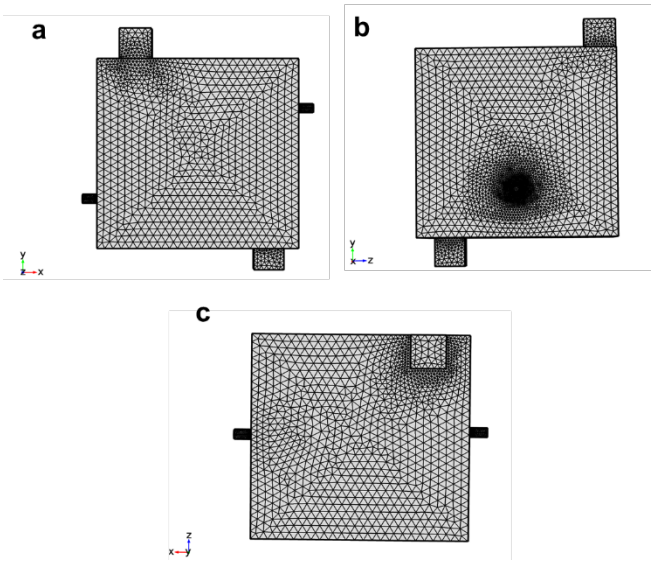

Figure 3. *Mesh element distribution on front (a), side (b), and bottom (c) of the chamber.*

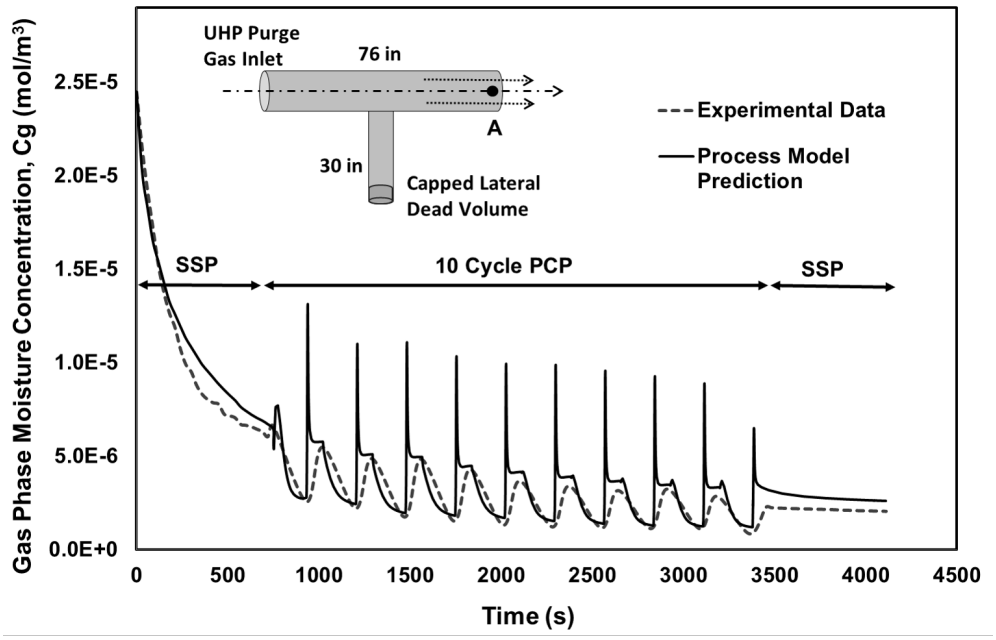

Figure 4. *Estimation of the input parameters by fitting the model to the data of PCP process in pipes [7]*

3.2 Comparison of PCP and Conventional SSP Purge Processes

The results for the chamber purge using both SSP and PCP are shown in Figure 5. The plot shows the gas-phase concentration at point A inside the chamber as well as the pressure cycle during the two purge schemes.

The key difference between the PCP and SSP can be illustrated by comparing the magnitude of gas velocity at two points (Center of the chamber and inside the dead volume) under these two purge methods as shown in Figure 6. As expected, the velocity at the center of the chamber is much higher than in the dead spaces indicating slower purging. However, during PCP, a relatively large transient component of gas velocity is generated which

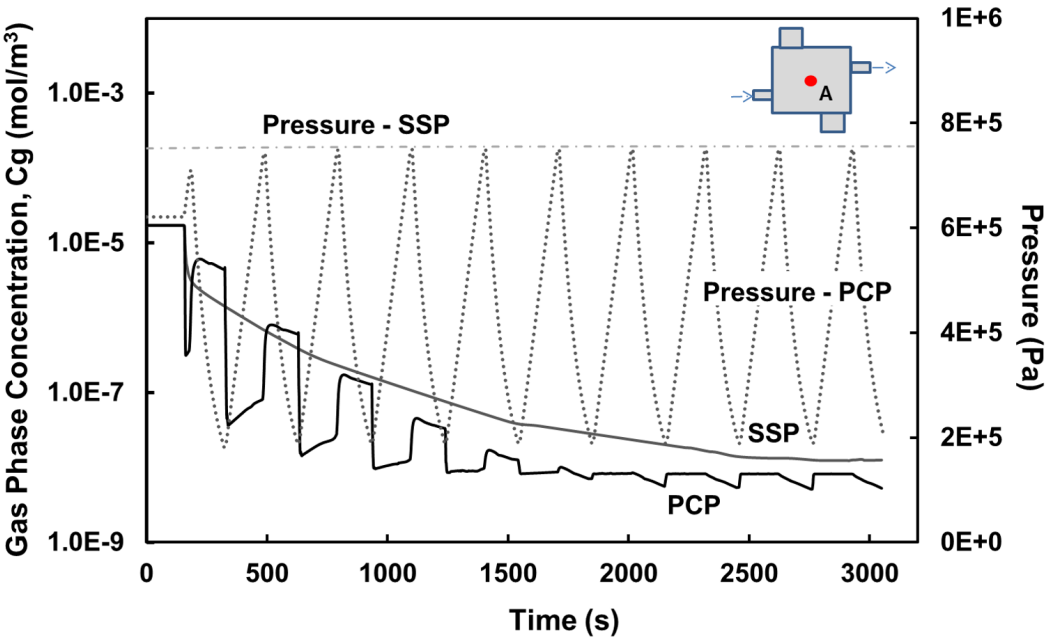

Figure 5. *Comparison of SSP and PCP chamber cleaning*

creates a beneficial convective mixing in the dead space. This effect is not observed in SSP where the overall gas velocity is lower than that of PCP.

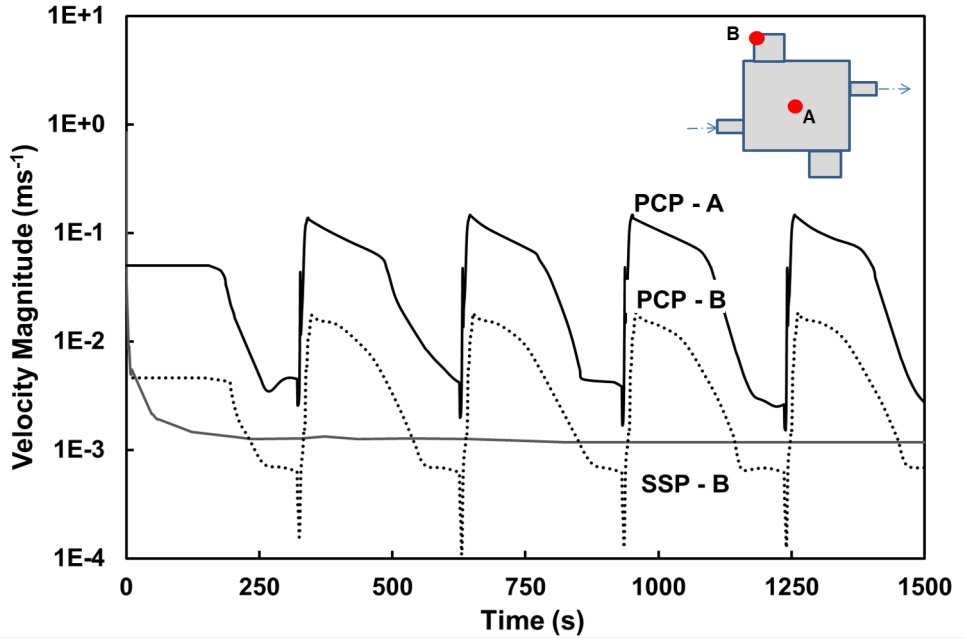

Figure 6. *Purge velocity profiles during SSP and PCP*

The temporal profiles of molar out-flux during SSP and PCP are shown in Figure 7. This flux, representing the average value over the outlet cross sectional area, decreases with time as purge proceeds and reaches a plateau

as the purge process approaches a desorption-controlled process. The small peaks in gas phase concentration are due to rapid pressurization. However, the overall pressure gradient is negligible since the propagation of pressure change in such small systems is very fast [15].

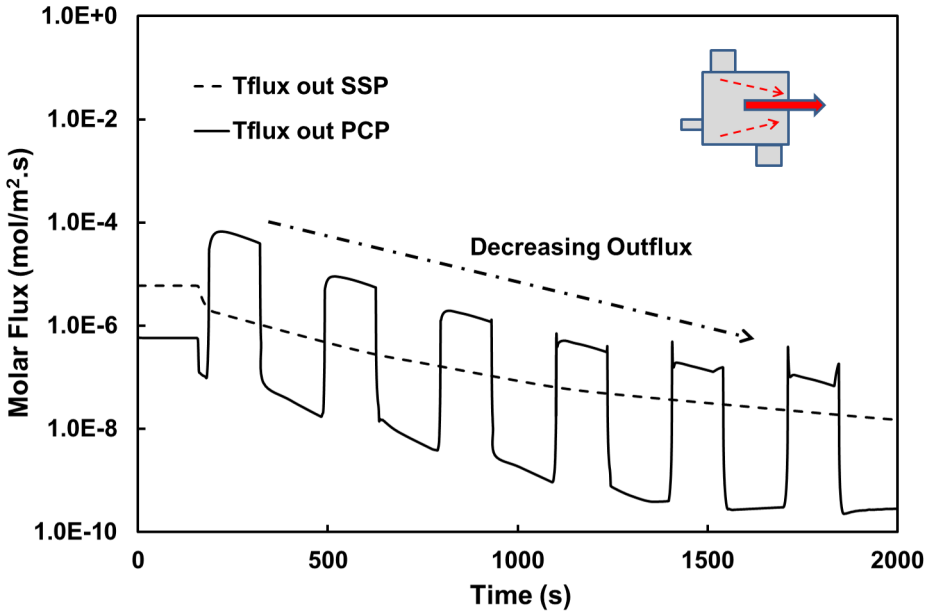

Figure 7. *Molar out-flux profiles during SSP and PCP*

Figure 8 gives the velocity distribution during pressurization and depressurization in different *xy* planes in the chamber. The magnitude of velocity in the figures can be inferred from the size of the vectors at a specific region. While depressurization promotes venting through out-flux of contaminants, re-pressurization allows mixing and dilution of gas phase through introduction of fresh UHP gas.

3.3 Comparison of PCP and SSP in Surface Cleaning

To demonstrate the cleaning, separately from the effect of partial pressure variations on gas concentration, surface concentration profiles were obtained as a metric of cleanliness of the chamber. Figure 9 shows the surface concentrations at points A and B located in top and bottom corner of the dead spaces, as shown in the schematic. The results show that PCP is more efficient than the conventional SSP in cleaning of both the gas phase and the surface. A larger difference between the two schemes can be seen at point A compared to point B. This is further explored in Figure 10 where cleaning of three points A, B, C are compared. The top dead space experiences the slowest purging due to the lower convection in that location, as seen in Figure 8.

Figures 9 and 10 show the variation in cleaning regime over time/number of pressure cycles. In order to explore the cleaning mechanism associated with individual pressure steps, the magnified details of surface concentration profile and gas contaminant outflux are shown in Figure 11 and 12 respectively. Figure 11 shows a few steps in PCP purge at a point inside the dead space (potentially the most difficult location to purge and clean). A rapid drop in surface concentration was observed during pressurization. This is due to introduction of UHP purge gas which lowers the gas-phase concentration and enhances the net desorption. The relatively small change in gas and surface concentrations during depressurizations is primarily due to the venting of contaminated gas. The out flux due to this venting action is shown in Figure 12.

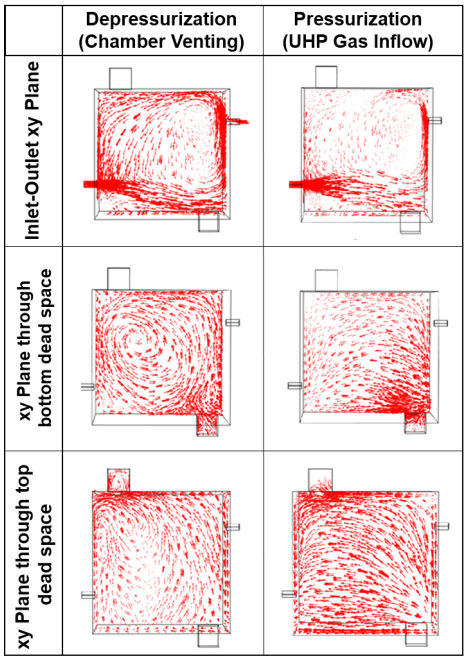

Figure 8. *Velocity distribution during depressurization and re-pressurization: a & b for cross section through inlet and outlet; c & d for cross section plane through bottom dead space; e & f for cross section plane through top dead space.*

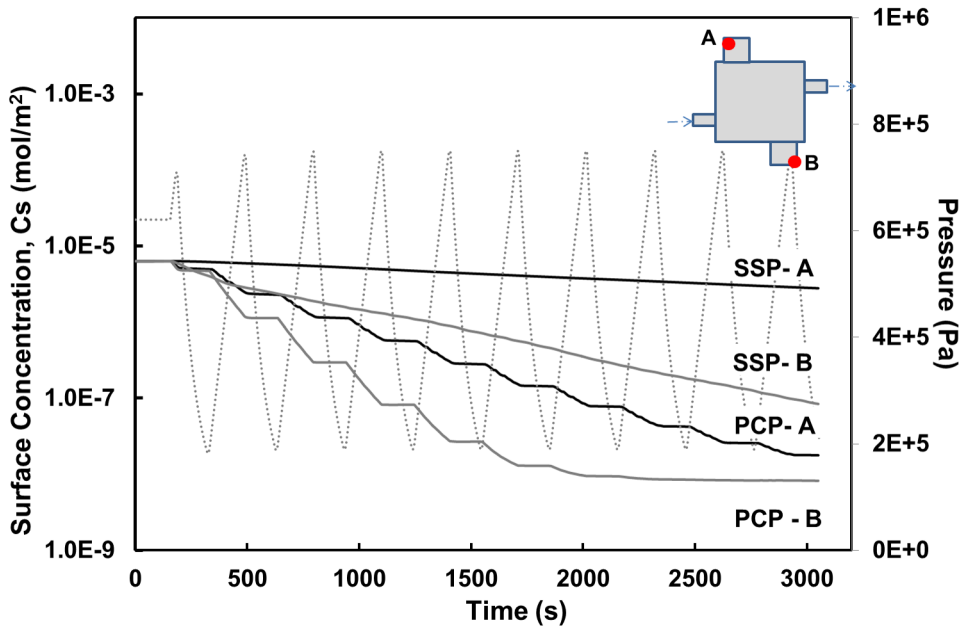

Figure 9. *Comparison of PCP and SSP in cleaning the surfaces of dead spaces.*

3.4 PCP Cycle Pressure Range

The operating pressure range for PCP is a major factor affecting the purge performance. To study this effect, the base case chamber was purged with PCP using two different cycle pressure ranges going from high pressure

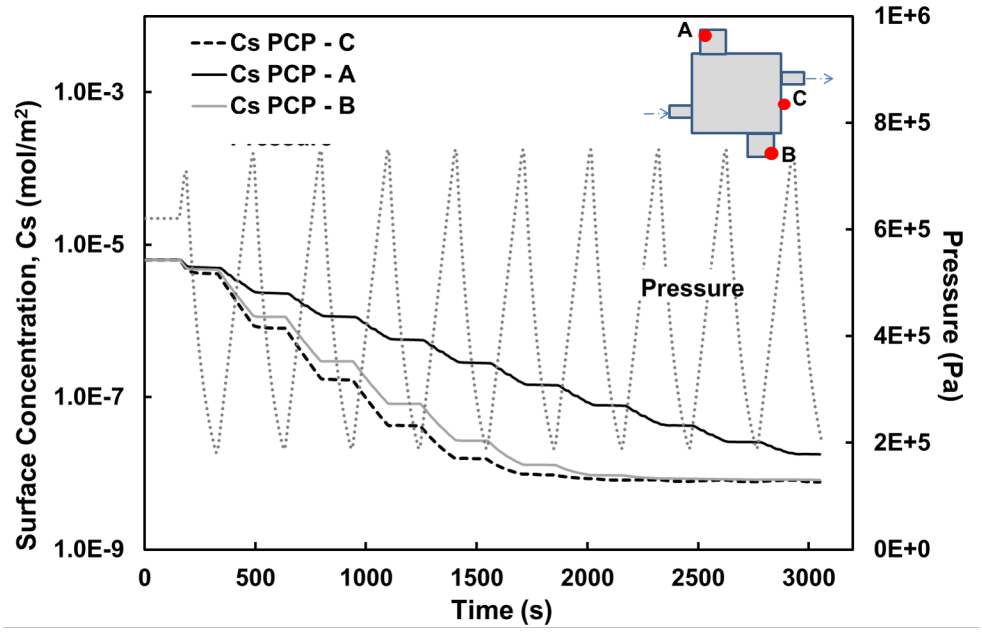

Figure 10. *Surface cleaning profiles at three locations in the chamber during PCP process.*

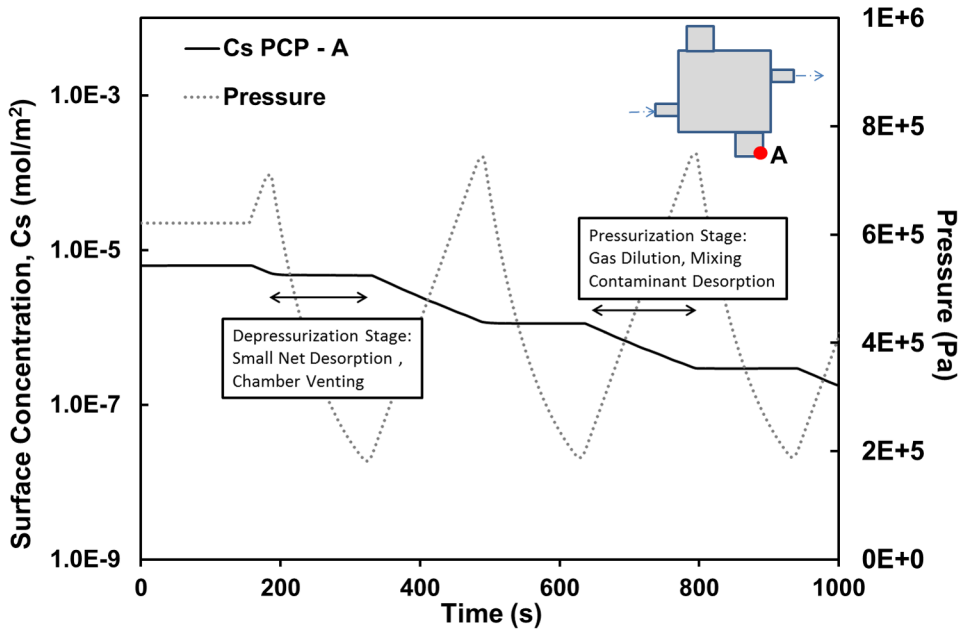

Figure 11. *Surface clean-up in a dead space by the PCP process.*

levels of 8.8*E*5 *Pa* and 7.5*E*5 *Pa* to the same low pressure level of 2*E*5 *Pa*. This created a cycle pressure range of 6.8*E*5 *Pa* and 5.5E5 Pa, respectively. Typically, a higher pressure range would require longer pressurization and depressurization times during each cycle. Figure 13 shows the time profile of cleaning the surface concentration at a point in the dead space corner using these two cycle pressure ranges. A faster cleaning is observed with a larger cycle pressure range.

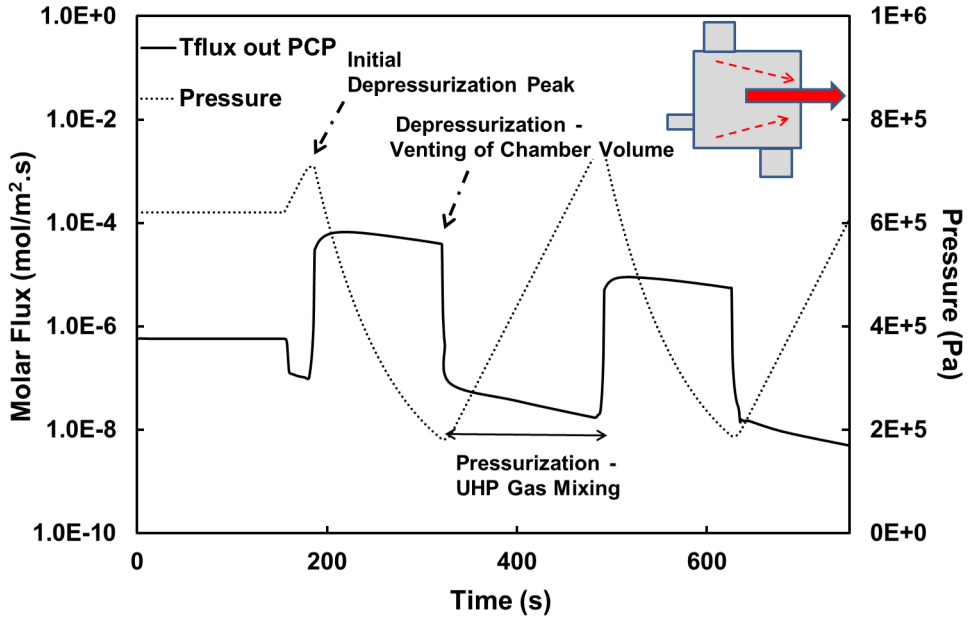

Figure 12. *Correlation of contaminant molar outflux and cyclic pressure stages.*

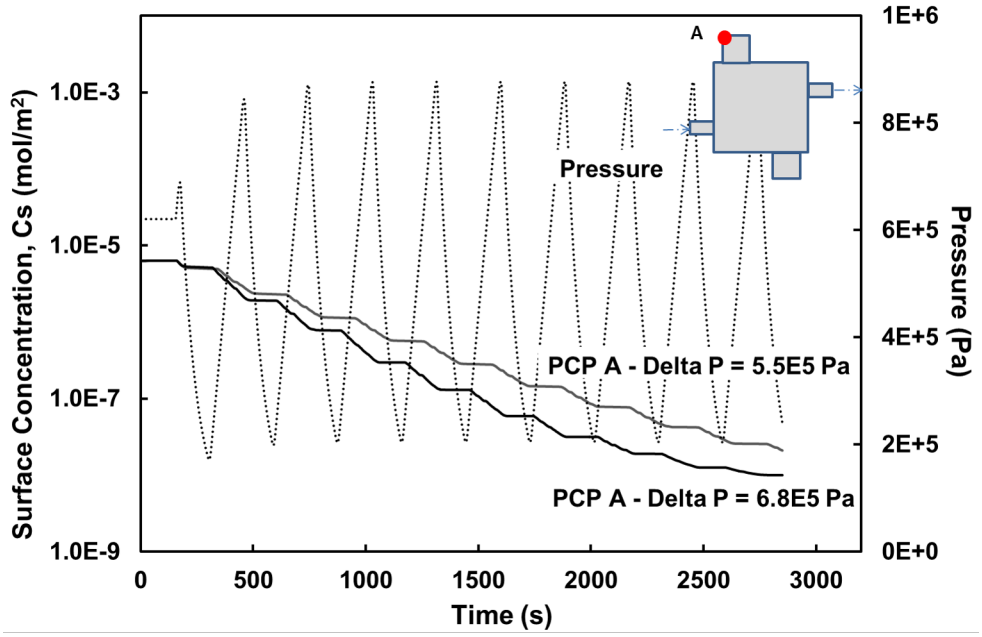

Figure 13. *The effect of cyclic pressure range on purge rate during PCP.*

A higher magnitude of molar flux and faster cleaning are achieved with a higher pressure range, as shown in Figure 14. This is primarily due to the fact a larger volume of contaminated gas is vented out with the increase in pressure cycle range. Increasing pressure range in PCP may not be beneficial beyond a certain point where the chamber size is small enough for process to become desorption controlled after a few cycles.

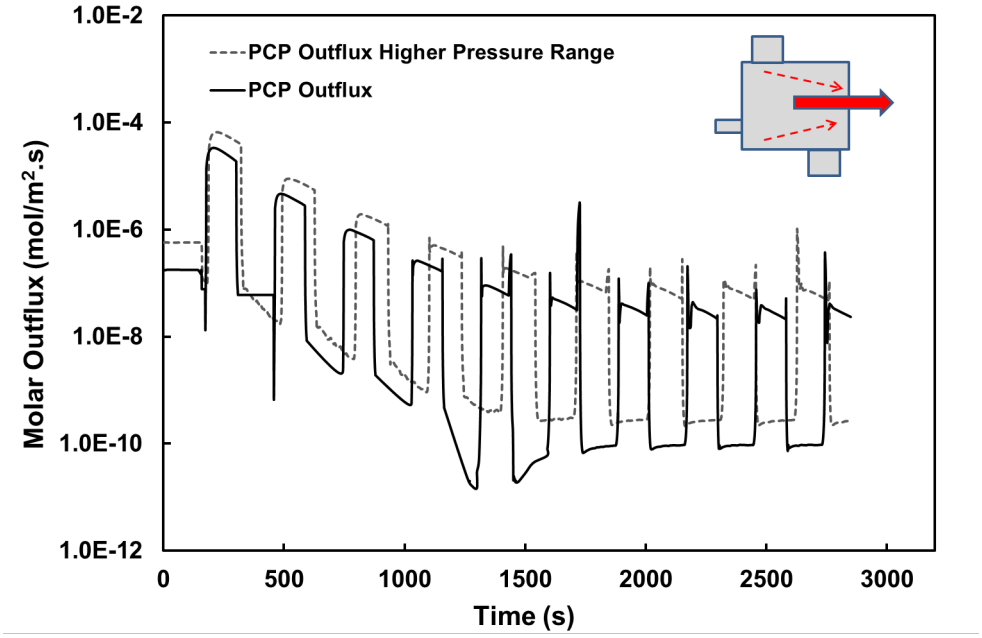

Figure 14. *Dependence of molar outflux on cycle pressure range during PCP.*

3.5 Chamber Shape

The chamber geometry also affects the optimum purge conditions. The purge performance on cylindrical and cubical chambers without dead spaces is compared when these chambers are purged with identical PCP scheme. The cylindrical chamber dimensions of length 1.24 m and diameter 0.36 m was chosen such that its total surface area and volume are similar to the cubical chamber. The inlet and outlet pipes are located off center with the same dimensions as in the base case geometry and similar path lengths. Figure 15 shows a comparison of the overall surface-averaged contaminant concentration for these two chambers. The total average surface concentration, $Avg\,C_s$ at any given point during the purge process is calculated by Equation (3.1):

$$Avg\,C_s = \frac{1}{A}\int C_s dA \tag{3.1}$$

where A is the total surface area of each chamber. Although a similar final cleanliness level is reached, the purge rates were different for the two geometries. This is due to fact that the dynamics of surface cleaning during PCP depends on the fluid flow conditions which are influenced by chamber geometry.

The purge time and gas usage needed to reach a certain level of cleanliness can be used as metrics to quantify the benefit of using PCP over SSP. Figure 16 shows the ratio of purge gas or purge time used in PCP to that used in SSP in order to reach a certain fractional surface cleanup target. The fractional surface cleanup is expressed by the ratio of the surface concentration to the initial surface concentration. The x axis in the Figure represents the fractional surface cleanup averaged over the total surface of the chamber, where the fractional surface cleanup is expressed according to Equation (3.2). The results show the purge time and gas savings by PCP compared to that SSP.

$$\text{Fractional Surface Cleanup} = \frac{C_{s0} - Avg\,C_s}{C_{s0}} \tag{3.2}$$

At low cleanup targets and small number of cycles, the PCP advantage is very large. At higher clean-up

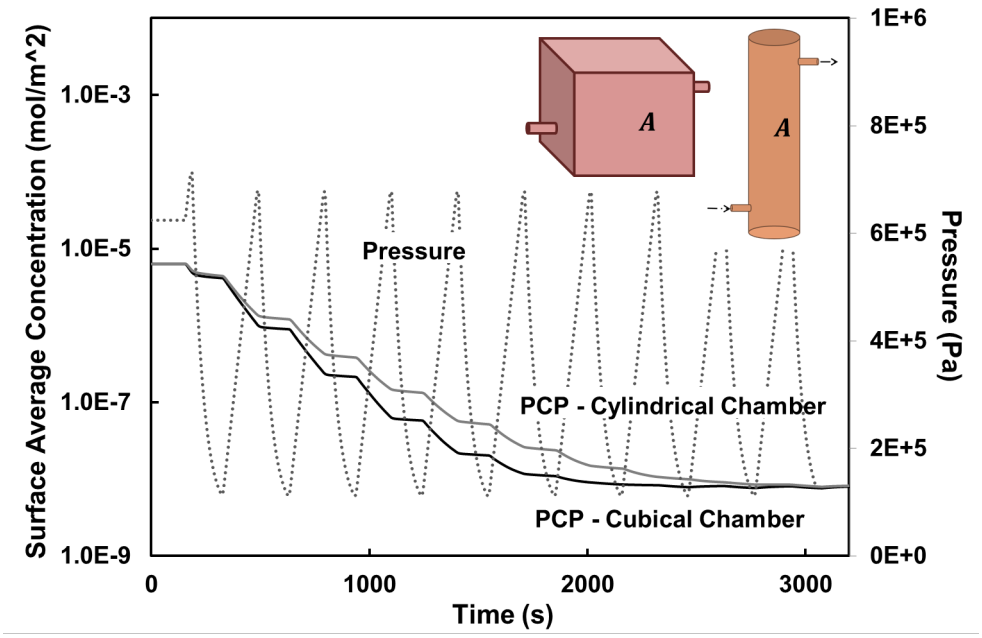

Figure 15. *The effect of chamber geometry on the overall surface cleaning during PCP process.*

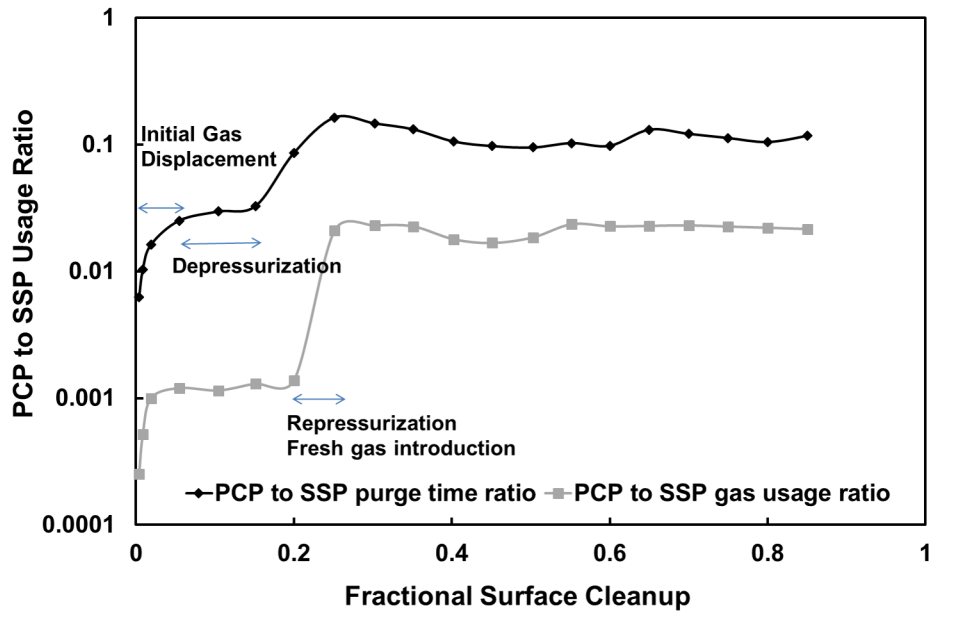

Figure 16. *Comparison PCP and SSP in terms of purge gas usage and required purge time.*

targets and large number of cycles, the time and usage ratios level off. The leveling of the ratios is due to a shift in purge mechanism towards a desorption- controlled process.

4. Conclusion

The conventional Steady State Purge (SSP) method is typically very inefficient and wasteful in time and purge gas usage for complex systems such as chambers with stagnant region and cavities. Through development and

application of a comprehensive process simulator, this study has shown the advantages of using a Pressure Cyclic Purge (PCP) method for removal of contaminant in complex chambers. The simulator can be used for studying the effect of various operational parameters, estimating the gas usage and cleaning time, and comparing various purge schemes.

The results show the significant advantages of the PCP process over the conventional SSP. This advantage is due to gas-phase dilution during pressurization, chamber venting during depressurization, and the enhanced transport and removal of contaminants due to convective flow generated by pressure cycles. The PCP-generated convective flow is particularly important in stagnant spaces since the impurity removal in the stagnant regions during conventional purge is only by diffusion which is a very slow process. The advantage of PCP over SSP increases as the complexity of the chamber increases; the gain is also higher for larger pressure range.

The simulator can be used to predict the purge gas and purge time required to reach a certain cleanliness target for a given chamber geometry. This capability is useful for developing efficient purge schemes in existing systems as well as in the design of new systems that require rapid and efficient purge.

Acknowledgments

Financial support from SRC Engineering Research Center for Environmentally Benign Semiconductor Manufacturing (SRC 2001-mc-425), Intel Corporation, and Arizona TRIF funds is acknowledged.

References

[1] PEARLSTEIN, Ronald M., BERGER, Kerry R., HARTZ, Christopher L., et al. Evaluating electronics-grade gas-line purging requirements. *Solid State Technology*, 2001, vol. 44, no 3, p. 119-119.

[2] DHEANDHANOO, Seksan, YANG, James, CIOTTI, Ralph, et al. Empirical validation of a gas distribution system moisture drydown model. *Journal of the IEST*, 1998, vol. 41, no 2, p. 33-38.

[3] DHEANDHANOO, Seksan, YANG, James H., et WAGNER, Michael D. Modeling the characteristics of gas system dry-down. *Solid State Technology*, 2001, vol. 44, no 6, p. 125-125.

[4] KUBUS, J. M. et LEGGETT, G. H. Piping system drydown predictions with field verification. In : *Microcontamination Conference Proceedings*. 1993. p. 212-221.

[5] YANG, Tian-Shiang, WU, Chuan-Hsieh, et YEH, Chia-Feng. Analysis of moisture purge in high purity gas distribution systems. *International journal of heat and mass transfer*, 2006, vol. 49, no 9, p. 1753-1759.

[6] YAO, Junpin, WANG, Hao, DITTLER, Roy, et al. Application of pressure-cycle purge (PCP) in dry-down of ultra-high-purity gas distribution systems. *Chemical Engineering Science*, 2010, vol. 65, no 17, p. 5041-5050.

[7] KISHORE, Jivaan, SHADMAN, Farhang, DITTLER, Roy, et al. Pressure cycling for purging of dead spaces in high-purity gas delivery systems. *AIChE Journal*, 2015, vol. 61, no 11, p. 3973-3980.

[8] VERMA, Nishith K., HAIDER, Asad M., et SHADMAN, Farhang. Contamination of Ultrapure Systems by Back-Diffusion of Gaseous Impurities. *Journal of the Electrochemical Society*, 1993, vol. 140, no 5, p. 1459-1463.

[9] DITTLER, Roy, KISHORE, Jivaan, GEISERT, Carl, et al. Contamination of ultra-high-purity (UHP) gas distribution systems by back diffusion of impurities. *Journal of the IEST*, 2014, vol. 57, no 1, p. 63-76.

[10] PANTON, Ronald L. *Incompressible flow*. John Wiley & Sons, 2006.

[11] BRODKEY, Robert S. et HERSHEY, Harry C. *Transport phenomena: a unified approach*. Brodkey publishing, 2003.

[12] SIEFERING, Kevin L. et WHITLOCK, Walter H. Measurement and modeling of moisture adsorption properties of 316 stainless steel tubing samples. *Journal of Vacuum Science & Technology* A, 1994, vol. 12, no 5, p. 2685-2691.

[13] MANAUL, Engineer. Engineering and Design; Liquid Process Piping. *Washington DC, US: US Army Corps of Engineers*, 1999.

[14] MULTIPHYSICS, COMSOL. COMSOL Multiphysics Reference Manual. 2013.

[15] GAKHELADZE, L. R., GELASHVILI, G. V., MDIVNISHVILI, M. O., et al. Shock wave propagation in gases under subatmospheric pressure. *Czechoslovak journal of physics*, 1999, vol. 49, no 6, p. 993-997.

Appendix

Nomenclature

a	Empirical constant dependent on chamber geometry
C_g	Gas phase concentration, $mol\ m^{-3}$
C_{gi}	Initial gas phase concentration in equilibrium with moisture in surface, $mol\ m^{-3}$
C_{gin}	Inlet gas phase concentration of UHP purge gas, $mol\ m^{-3}$
C_s	Surface moisture concentration, $mol\ m^{-2}$
C_{s0}	Initial surface concentration in equilibrium with gas phase contaminant, $mol\ m^{-2}$
D_e	Effective dispersion coefficient, $m^2\ s^{-1}$
D_m	Molecular diffusion coefficient of contaminant in N_2 at atmospheric pressure P_{atm}, $m^2\ s^{-1}$
D_{mp}	Molecular diffusion coefficient of contaminant in N_2 at pressure p, $m^2\ s^{-1}$
D_s	Surface diffusivity of contaminant on $316L$ EPSS, $m^2\ s^{-1}$
d	Diameter of inlet pipe to the chamber under purge, m
k_a	Rate constant for adsorption of contaminant on EPSS, $m^3\ mol^{-1}\ s^{-1}$
k_d	Rate constant for desorption of contaminant on EPSS, s^{-1}
K_f	Characteristic valve loss coefficient
M_n	Molecular Weight of N_2, $0.028\ kg/mol$
n	Unit normal vector pointing outward from the chamber surface
p	Pressure, Pa
P_{atm}	Atmospheric Pressure, Pa
P_{st}	Standard pressure, 101325 Pa
Q_{in}	Periodic function for inlet mass flow rate, $sccm$
R	Universal gas constant, $8.314\ J\ mol^{-1}\ K^{-1}$
S_0	Density of active surface site, $mol\ m^{-2}$
t	Time, s
t_d	Duration of depressurization stage, s
t_p	Duration of re-pressurization stage, s
T_{st}	Standard temperature, K
u	Gas velocity in experimental test bed, $m\ s^{-1}$
W	Length of chamber edge, m

Greek Letters

μ	Dynamic viscosity of UHP gas, $Ns\ m^{-2}$
ρ	Density of UHP gas, $kg\ m^{-3}$
ρ_{st}	Density of the gas at standard conditions, $kg\ m^{-3}$

Abbreviations

EPSS	Electro polished stainless steel
ESH	Environmental Safety and Health
MFC	Mass Flow Controller
PCP	Pressure cyclic purge
SSP	Steady-state purge
UHP	Ultra-high purity
ppb	Parts per billion
ppt	Parts per trillion
sccm	Standard cubic centimeters